

Chemical Science

Accepted Manuscript

This article can be cited before page numbers have been issued, to do this please use: J. Qin, Y. Yin, X. Guan, X. Ge, M. Cao, J. Ouyang and N. Na, *Chem. Sci.*, 2025, DOI: 10.1039/D5SC02194D.



This is an Accepted Manuscript, which has been through the Royal Society of Chemistry peer review process and has been accepted for publication.

Accepted Manuscripts are published online shortly after acceptance, before technical editing, formatting and proof reading. Using this free service, authors can make their results available to the community, in citable form, before we publish the edited article. We will replace this Accepted Manuscript with the edited and formatted Advance Article as soon as it is available.

You can find more information about Accepted Manuscripts in the [Information for Authors](#).

Please note that technical editing may introduce minor changes to the text and/or graphics, which may alter content. The journal's standard [Terms & Conditions](#) and the [Ethical guidelines](#) still apply. In no event shall the Royal Society of Chemistry be held responsible for any errors or omissions in this Accepted Manuscript or any consequences arising from the use of any information it contains.

ARTICLE

Revealing Axial-Ligand-Induced Switching of Spin States for Controllable Single Electron Transfer-based Radical Initiation†

Jingyi Qin,^a Yiyan Yin,^a Xiaowen Guan,^a Xiyang Ge,^a Mengyu Cao,^a Jin Ouyang,^b Na Na^{*a}Received 00th January 20xx,
Accepted 00th January 20xx

DOI: 10.1039/x0xx00000x

Radicals are highly reactive for coupling reactions while the applications are normally limited by the uncontrollable initiation and chaotic conversions. Although transition metal-based single electron transfer (SET) shows potential for controllable radical initiations, the detailed mechanism is still insufficient, especially for the roles of spin state transition on SET-based radical initiation. Herein, with Fe(III)-catalyzed thiol-ene click (TEC) reaction as an example, the axial-ligand-induced switching of transition metals' spin states was revealed to facilitate controllable SET-based radical initiation and the subsequent coupling reactions. Given the advantages of the on-line monitoring by ambient mass spectrometry (AMS), the short-lived radical intermediates and their dynamic changes were explored. As demonstrated, initiated by the axial coordination of sulfhydryl with Fe(III)-porphyrin, the selective generation of thiyl radical (RS•) via SET was achieved. Besides, as another axial-ligand, O₂ in air was coordinated to Fe(III)-porphyrin, inducing the conversion of Fe(III) from high spin (S = 5/2) to low spin state (S = 1/2). This lowered the energy barrier for SET-based radical initiation, further facilitating the final selective coupling with vinyl reactant. Upon revealing the axial-ligand-induced switching of the spin states by AMS and other examinations, rational design of transition metal catalysts would be promoted for efficient and highly selective radical reactions.

Introduction

Radicals have attracted much attention for their advantages of reacting with most organic molecules including sterically hindered molecules and those hard to be synthesized by catalytic reactions.^{1–3} Especially, with high reactivity and unique properties, radicals are expected to initiate rapid coupling to construct complex heterocyclic compounds.^{4–5} However, the highly active radical species would normally cause unfavourable chaotic, uncontrollable, and mysteriously baffling processes.^{6–8} Consequently, effective strategies for the controllable generation of radicals for chain initiation, as well as the subsequent directional conversion for chain propagation are crucial for efficient radical synthesis.

For radical reactions, transition metal catalysis has been regarded as one of the versatile platforms.^{9–13} Taking advantage of unpaired d-electrons, transition metals normally possess unoccupied orbitals to undergo single electron transfer (SET) to generate radicals.^{9, 14} Significantly, upon modulating the coordination environments of transition metal sites, the spin state-related electron transfer could accelerate reaction kinetics by lowering the activation energy barrier.^{15–17} Predictably, the radical initiation via SET could be modulated

by spin states. While the current modulation of spin states normally focuses on rearrangement of d-electron orbitals to enhance inorganic catalytic reactions.^{18–21} There is still short of report to reveal roles of transition metals' spin states on electron transfer-based radical initiation, thereby hindering the efficient radical initiation by metals.

For instance, aryl sulfide radicals can be initiated in the metal-catalyzed thiol-ene click (TEC) reaction, which facilitated C–S coupling to exhibit significance in pharmaceuticals and chemical engineering.^{22–26} Nevertheless, the initiation of various active species is usually non-selective due to the wide potential range of transition metals. Consequently, the mechanism of controllable radical reactions is worth exploring in detail.^{27–29} Unfortunately, although the radical directional conversion (chain propagation) was examined, there is still short of clear description on SET-based radical initiation, not to mention roles of spin states for this initiation (Scheme 1a).^{8, 12, 30–31} This could be largely limited by the difficulties on obtaining dynamic conversions of reactive radicals or intermediates with short lifetime.^{32–35} More importantly, revealing the clear relationship between SET and spin-state switching is comprehensive and challenging, which requires detailed studies of the reaction process including the coordination behaviours of catalysts. Consequently, more efforts are encouraged to reveal the effect of spin states on the SET-based radical initiation.

Herein, to examine effects of spin states on controllable initiation of free radicals via SET, the TEC reaction of thiophenol and styrene was selected as the model reaction (Scheme 1b). Controllable generation of thiyl radical (RS•) was

^a Key Laboratory of Radiopharmaceuticals, Ministry of Education, College of Chemistry, Beijing Normal University, Beijing 100875, China. E-mail: nana@bnu.edu.cn

^b Department of Chemistry, Faculty of Arts and Sciences, Beijing Normal University, Zhuhai 519087, China.

† Electronic supplementary information (ESI) available. See DOI: 10.1039/x0xx00000x



catalyzed by Fe(III)-porphyrin, which could be attributed to SET from sulfhydryl to Fe(III). To examine dynamic conversions of reactive radicals or intermediates with short lifetime, an ambient mass spectrometry (AMS) was constructed for online monitoring, achieving rapid structural identifications without sample pretreatments.³⁶⁻³⁹ Based on the comprehensive characterizations, axial coordination of sulfhydryl with Fe(III)-porphyrin was confirmed to be crucial for the selective SET process. Moreover, O₂ was revealed to act as another axial-ligand to bind with the sulfhydryl-Fe(III)-porphyrin complex, triggering the conversion of Fe(III) from high spin (*S* = 5/2) to low spin (*S* = 1/2) state. This lowered the energy barrier of radical generation via SET, leading to the acceleration of reaction in air. Furthermore, upon coordination with Fe(III)-porphyrin, the controllable radical initiation by SET would be facilitated by substrates with higher electron-donating abilities. This work has enabled the AMS techniques for in-depth examination of controllable SET-based radical initiation, which would promote developments of transition metal catalysts for efficient and selective radical reactions.

Results and Discussion

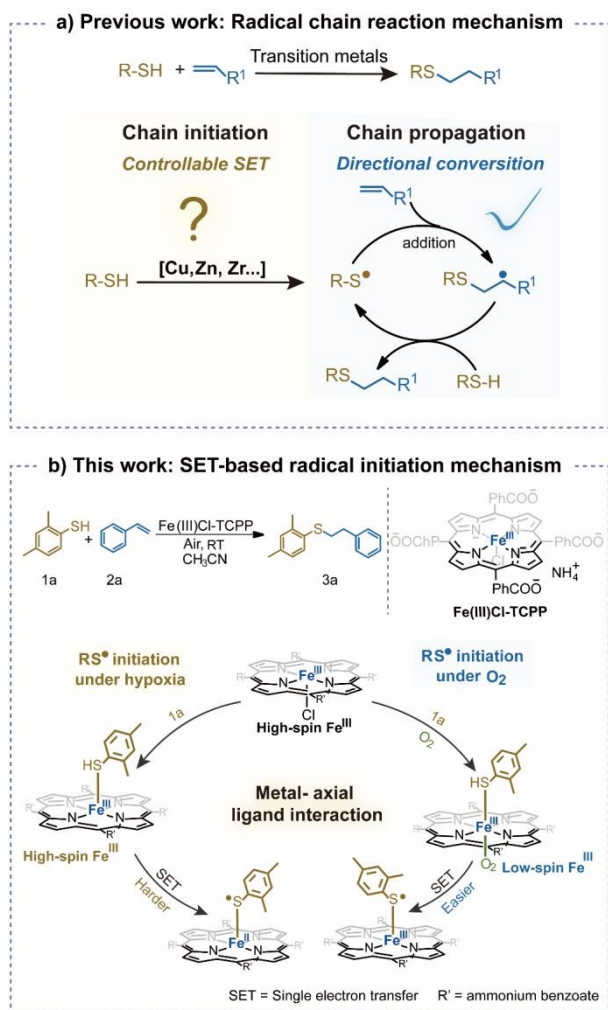
View Article Online

DOI: 10.1039/D5SC02194D

Evaluation of radical initiation in TEC reaction

In the present TEC reaction, the C-S coupling of reactants 2,4-dimethylbenzenethiol (**1a**) and styrene (**2a**) was catalyzed by transition metal catalyst of Fe(III)Cl-TCPP (Figure S1). For the rapid evaluation of TEC performance, the reaction system was directly detected by the AMS. As shown in Figure 1a, the reaction solution was extracted and ionized by a high-velocity (sonic) nebulizing stream of N₂ gas through an external capillary. In this way, the samples in the reaction system can be directly monitored without sample pre-treatments, which enabled the revealing of important short-lived intermediates. As monitored (Figure 1b), the significant product ion of [3a+H]⁺ at *m/z* 243 was observed after reacting for 5 min. It should be noted that the relatively low abundance of disulfide at *m/z* 275 and sulfoxide at *m/z* 259 were observed, identified by collision induced dissociation (CID) analysis and HR-MS (Figure S2-3). This indicated the highly selective generation of the product of C-S coupling, in accordance with the NMR evaluations (Figure S18-1).

Subsequently, to confirm the radical initiation of TEC, the radical scavenger of 2,2,6,6-tetramethyl piperidine-1-oxyl (TEMPO) was added into reaction system for AMS detections. As resulted (Figure 1c), no significant product signal of [3a+H]⁺ (*m/z* 243) was recorded. While the main ion peak at *m/z* 398 was exhibited, attributed to the coupling of the carbon radical intermediate (the precursor of the product **3a**) with TEMPO. The corresponding structure was confirmed by collision induced dissociation (CID) experiments (Figure S4). Consequently, the radical intermediate was captured by TEMPO, which greatly hindered the generation of the product **3a**. This indicated that the present transition metal-catalyzed TEC reaction involved stepwise radical conversions after the radical initiation.



Scheme 1. The illustration of transition metal-catalyzed thiol-ene click (TEC) reactions. (a) Radical chain reaction mechanism (previous work). (b) The mechanism of SET-based controllable radical initiation in Fe(III)-catalyzed TEC reaction under different conditions (this work).

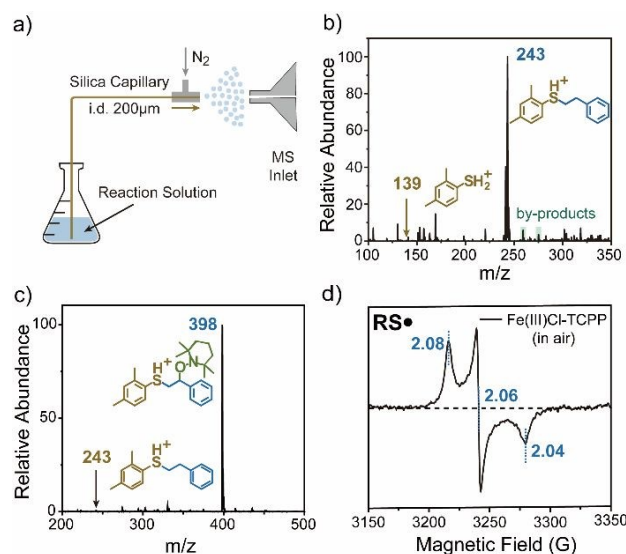


Figure 1. Evaluation of the radical initiation of TEC reaction. (a) Schematic diagram of AMS setup. (b) Mass spectrum of the reaction system for 5 min in air. Reaction conditions: **1a** (0.5 mmol), **2a** (0.5 mmol) and Fe(III)Cl-TCPP (0.25 mol%) in 3 mL solvent (CH₃CN:H₂O=10:1, v/v). (c) Mass spectrum of the reaction system with radical scavenger of TEMPO added. (d) EPR spectrum of DMPO - RS[•] in the mixture of substrate **1a** and Fe(III)Cl-TCPP catalyst in air.



To further confirm the generation of radical intermediates in TEC, the mixture of substrate **1a** and catalyst Fe(III)Cl-TCPP was examined by EPR characterization with 5,5-dimethyl-1-pyrroline N-oxide (DMPO) as the trapping agent. The presence of RS• was verified by the EPR signals ($g = 2.08, 2.06$, and 2.04) (Figure 1d), which were attributed to the adduct of RS• and DMPO. This was also in accordance with the previous reports.⁴⁰ Besides, to further confirm the selective radical generation, other thiophenol substrates with various substituted groups were selected for employing TEC reactions. As expected, the highest yields were obtained for the substrates with benzene-ring bearing electron-donating groups (92% of **3a** for -Me, 94% of **3b** for -OMe) (Figure S5).

While the substrates with electron-withdrawing groups afforded lower product yields (65–81% of **3c–3e** for -Cl, -CF₃, and -NO₂). These reaction products were verified by NMR characterizations (Figure S18–2 to 4). Consequently, the efficient radical initiation can be obtained with higher electron-donating abilities of substrates. In addition, the highest yield was obtained for the TEC in acetonitrile (CH₃CN) and dichloromethane (DCM) (entries 1–2), much higher than in methanol (CH₃OH) with the strongest coordination ability (entry 3) (Figure S6). This can be deduced that the coordination is crucial for radical initiation. Consequently, the RS• was selectively generated in the TEC process, which played an important role for the subsequent C-S coupling at high-yield.

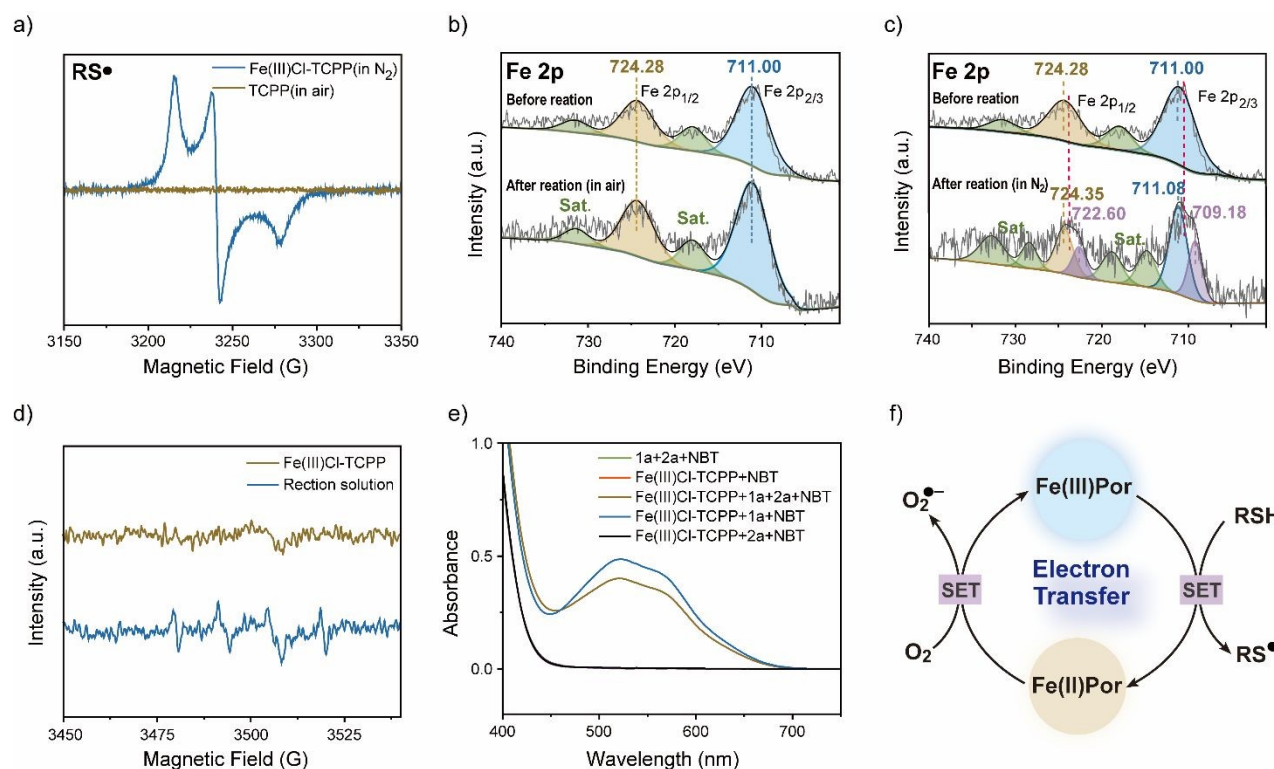


Figure 2. Examinations of radical generation upon SET process. (a) EPR spectra of the mixture of substrate **1a** and Fe(III)Cl-TCPP in N₂ (blue line) or the mixture of **1a** and TCPP in air (yellow line). (b) XPS spectra of Fe 2p before and after TEC reaction in air. (c) XPS spectra of Fe 2p before and after TEC reaction in N₂. (d) DMPO-O₂• signals for catalyst and reaction system. (e) UV-vis absorption of NBT colorimetric reaction with O₂• in different systems. (f) Proposed mechanism of O₂ and Fe(III)Por involved SET-based radical initiation.

Examination of radical generation upon SET process

As proposed, RS• could be generated via SET between the sulfide substrate and transition metals or O₂.^{29, 41} In this way, further efforts are required to clear the real process of the present radical initiation upon electron transfer between **1a** and Fe(III)Cl-TCPP or O₂. To examine the generation of RS• upon SET, the roles of O₂ and Fe(III) were firstly evaluated by EPR analysis under different conditions. For the mixture of **1a** and Fe(III)Cl-TCPP, EPR signals of RS• were still obvious even in N₂ (blue line, Figure 2a), which were similar to that in air. While without Fe(III), no radical signal was recorded in the TCPP system (yellow line, Figure 2a). This was in accordance with the low yield of TEC without Fe(III) active species in the catalyst (Figure S7). Furthermore, the highest yield was recorded in the O₂ environment, a little higher than that in N₂ (Figure S7).

Consequently, it can be deduced that the transition metal of Fe(III) played an important role in the radical initiation, while O₂ was not the essential factor but can facilitate the generation of RS•.

To further examine the roles and changes of Fe(III)Cl-TCPP in the TEC reaction, chemical states of iron ion in air and N₂ were evaluated by X-ray photoemission spectroscopy (XPS). In air (Figure 2b), the XPS peaks of Fe(III) (at the binding energies of 724.3 and 711.0 eV)^{42–43} were observed before and after the reaction. This demonstrated the good stability of Fe(III)Cl-TCPP in TEC reaction, which was crucial for the highly efficient catalytic reactions. However, after the reaction in N₂ (Figure 2c), the significant XPS peaks of both Fe(III) (at 724.4 and 711.1 eV) and Fe(II) (at 722.6 and 709.2 eV)⁴⁴ were recorded. This indicated the employment of electron transfer in the Fe(III)Cl-TCPP-catalyzed TEC. Consequently, the reduction of Fe(III) to



Fe(II) could be achieved via SET from substrate **1** to Fe(III), along with the generation of RS[•]. Notably, no obvious signal of Fe(II) was observed in the reaction in air. This could probably

be attributed to the oxidation of the generated Fe(II) by O₂ in air, which generates Fe(III) for catalytic reactions in the next TEC reactions.

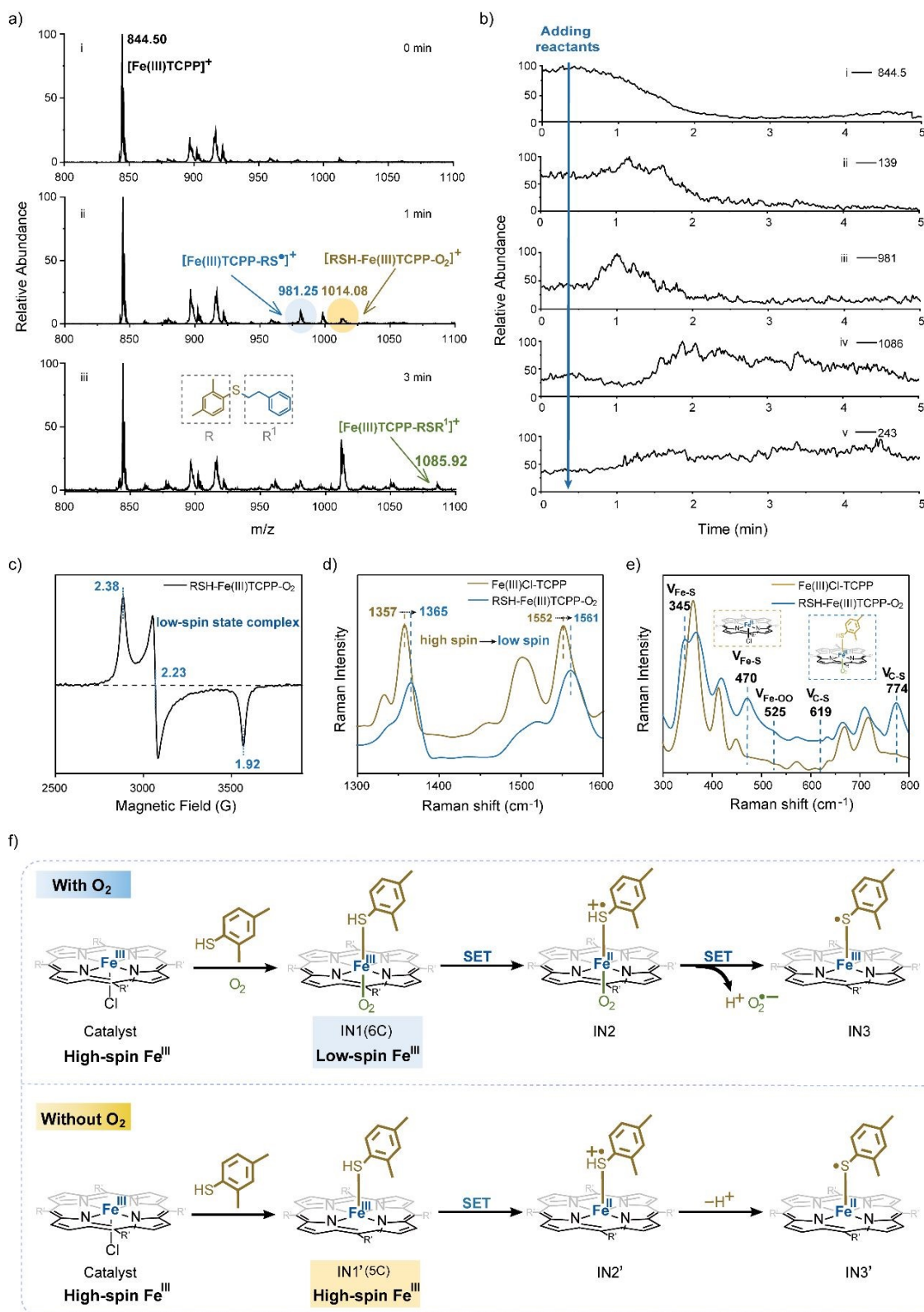


Figure 3. Examination of intermediates during SET-based radical initiation. (a) Detection of the reaction system by AMS at different reaction time (R=2,4-dimethylphenyl, R¹=phenylethyl). Reaction conditions: **1a** (0.5 mmol), **2a** (0.5 mmol) and Fe(III)Cl-TCPP (0.25 mol%) in 3 mL solvent (CH₃CN:H₂O=10:1, v:v). (b) Dynamic monitoring of different ions. EICs of [Fe(III)TCPP]⁺ at m/z 844.5 (i), [1a+H]⁺ at m/z 139 (ii), [Fe(III)TCPP-RS]⁺ at m/z 981.3 (iii), [Fe(III)TCPP-3a]⁺ at m/z 1085.9 (iv) and [3a+H]⁺ at m/z 243 (v). (c) EPR spectra of the intermediate **1** [RSH-Fe(III)TCPP-O₂]⁺. (d and e) Raman spectra of Fe(III)Cl-TCPP and intermediate **1** [RSH-Fe(III)TCPP-O₂]⁺. (f) Two possible reaction mechanisms for the selective generation of RS[•] at different atmospheres.



Subsequently, to further examine O_2 changes upon SET in TEC, the reactive oxygen species (ROS) were detected by EPR with DMPO as the radical trapping reagent. As shown in Figure 2d, no obvious ROS signal was recorded in the system of Fe(III)Cl-TCPP. While after TEC reaction for 1 min, the significant signal of DMPO- $O_2^{\bullet-}$ was observed,⁴⁵ demonstrating the transfer of an electron from Fe(II) to O_2 . In addition, the generation of $O_2^{\bullet-}$ was further evaluated by UV-vis absorption analysis, based on the absorption of blue formazan deposit (~520 nm) generated from the oxidation of nitro blue tetrazolium (NBT).⁴⁶⁻⁴⁷ As shown in Figure 2e, the strong absorption was recorded for substrate **1a** with Fe(III)Cl-TCPP added (blue line) and the TEC reaction system (yellow line). While no signal was observed in substrate **2a** with Fe(III)Cl-TCPP added. Consequently, it can be demonstrated that the electron transfers only occurred in the chain initiation process, rather than the chain propagation process. In fact, as shown in Figure 2f, an electron was transferred from substrate **1** to Fe(III)Cl-TCPP, generating RS^{\bullet} and Fe(II) species. Simultaneously, the electron transfer from Fe(II) to O_2 can be employed in air, along with the generation of $O_2^{\bullet-}$ in TEC. Consequently, this TEC involved two cascade SET processes for the generation of radicals of both RS^{\bullet} and $O_2^{\bullet-}$.

Capture and detection of intermediates during SET-based radical initiation

The intermediates corresponding to both catalyst and substrate were captured and examined by online AMS to elucidate the SET-based radical initiation for the selective RS^{\bullet} generation. As detected, the characteristic ion of catalyst $[Fe(III)TCPP]^+$ (m/z 844.5) was recorded in the reaction system at the beginning (Figure 3a-i). With the TEC reaction proceeding (at 1 min, Figure 3a-ii), the new ions of $[Fe(III)TCPP-RS^{\bullet}]^+$ (m/z 981.3) and $[RSH-Fe(III)TCPP-O_2]^+$ ($R = 2,4$ -dimethylphenyl) (m/z 1014.1) were observed. The corresponding structures were confirmed by HR-MS (Figure S8) and CID experiments (Figure S9). Besides, the deuterium substituted substrate **1a** was also applied to the TEC reaction to verify the structures. As resulted (Figure S10), the ions of $[Fe(III)TCPP-RS^{\bullet}]^+$ (m/z 981.2) and $[RSD-Fe(III)TCPP-O_2]^+$ (m/z 1014.9) were observed, which further confirmed the intermediate structures. While with the TEC reaction carried on, both intermediates of $[Fe(III)TCPP-RS^{\bullet}]^+$ (m/z 981.3) and $[RSH-Fe(III)TCPP-O_2]^+$ (m/z 1014.1) decreased (at 3 min, Figure 3a-iii). Interestingly, the new ion of $[Fe(III)TCPP-RSR^1]^+$ (R^1 =phenylethyl) (m/z 1085.9) was observed, which was attributed to the complex of product **3a** and catalyst. The corresponding structure was identified by CID experiment (Figure S11). Consequently, it can be deduced that the selective generation of RS^{\bullet} ($[Fe(III)TCPP-RS^{\bullet}]^+$) was related to the electron transfer within the intermediate of $[RSH-Fe(III)TCPP-O_2]^+$. Thereafter, another intermediate of $[Fe(III)TCPP-RSR^1]^+$ was obtained by the radical chain transfer along with the consuming of initial intermediates.

Subsequently, the dynamic changes of the intermediates and important species were examined by the online extracted ion chromatograms (EICs). As shown in Figure 3b (i to ii), the

reactant ion of $[1a+H]^+$ (m/z 139) and catalyst ion of $[Fe(III)TCPP]^+$ (m/z 844.5) decreased gradually. While the ion at m/z 981 ($[Fe(III)TCPP-RS^{\bullet}]^+$) increased gradually and reached a peak value within 1 min (Figure 3b-iii), indicating the successful generation of RS^{\bullet} . Thereafter, $[Fe(III)TCPP-RS^{\bullet}]^+$ came to decrease along with the simultaneous increase of chain propagation intermediate of $[Fe(III)TCPP-3a]^+$ (m/z 1086) and the final product of $[3a+H]^+$ (m/z 243) (Figure 3b-iv and v). Consequently, the dynamic changes of different species have confirmed the initially radical initiation, followed by the chain propagation along with RS^{\bullet} consumption to obtain the final product.

To further examine the coordination between substrates and the active site of Fe(III), the reaction intermediates were characterized by the EPR and Raman spectrometry. To avoid effects of solvent coordination on characterizations, the experiments were employed in the non-coordinating solvent of DCM. Firstly, the high-spin Fe(III) ($S = 5/2$) EPR signals of Fe(III)Cl-TCPP at $g=6.23, 4.29, 2.00$ were detected, but these signals vanished after reaction in N_2 (Figure S12).⁴⁸⁻⁴⁹ This confirmed the generation of Fe(II) (silent EPR signals) upon SET from substrate **1a** to Fe(III), in accordance with the XPS data (Figure 2c). Thereafter, the intermediates were examined by EPR analysis at low temperature, avoiding the rapid conversion of radical intermediates for better examinations. After adding substrate **1a** to Fe(III)Cl-TCPP in air (Figure 3c), the mixture was quickly frozen to $-80^{\circ}C$ to obtain the significant EPR signals of low-spin Fe(III) ($S = 1/2$) ($g=2.38, 2.23, 1.92$).⁵⁰ Given that the intermediate of $[RSH-Fe(III)TCPP-O_2]^+$ (IN1) was generated by the coordination of Fe(III)-porphyrin with substrate **1a** and O_2 (demonstrated in Figure 3a-ii), this intermediate could be assigned as the low-spin species.

The specific low-spin IN1 was further confirmed by low-temperature Raman spectrometry analysis. After adding substrate **1a** into catalyst system of Fe(III)Cl-TCPP in air (Figure 3d), the oxidation and spin state marker bands of ν_4 and ν_2 exhibited a blue shift (from 1357 to 1365 and 1552 to 1561 cm^{-1}). This indicated the formation of the low-spin structure for Fe(III)-porphyrin. In addition, some new peaks were observed in the low-frequency region (Figure 3e), attributed to Fe(III)-S stretching vibrations (345 and 470 cm^{-1}), Fe(III)-OO vibration (525 cm^{-1}) and C-S stretching vibrations (619 and 774 cm^{-1}).^{50, 51} Briefly, the intermediate of IN1 was generated upon the coordination of Fe(III) (in iron porphyrin) with S atom (in substrate **1**) and O atom (in oxygen). This was further confirmed by the following theoretical calculations. Therefore, the thiyl radical initiation exhibited the high selectivity, upon the restriction of electron transfer sites from substrate **1a** to Fe(III) by the coordination interaction.

Consequently, the mechanism of SET-based chain initiation can be proposed in Figure 3f. Initially, Fe(III)-porphyrin was coordinated with substrate **1a** and O_2 to afford a six-coordinate (6C) low-spin intermediate of $[RSH-Fe(III)TCPP-O_2]^+$ (IN1). Subsequently, upon the first SET process, the sulfhydryl of RSH transferred an electron to Fe(III) to generate the Fe(II)-complex (IN2), exhibiting the coordination of RS^{\bullet} and O_2 with Fe(II)-porphyrin. Notably, the structure of IN2 was similar to



the activated state of cytochrome P450 in biological system.⁵² This could activate O₂ to act as the final electron acceptor to oxidize Fe(II) via the second SET process. Therefore, the O₂^{•-} was generated along with the recovery of Fe(II) to Fe(III). However, in the absence of oxygen, the five-coordinate (5C) complex of [RSH-Fe(III)TCPP]⁺ (IN1') was also at high spin states, formed by the interaction between thiolate (weak field ligand) and Fe(III)-porphyrin, which was further confirmed by

the following theoretical calculations. Although the SET-based radical initiation was also employed, the catalyst failed to revert to its high valence state, thus impeding the continuous SET process with the substrate **1a**. Finally, the RS[•] was generated and coordinated with Fe(III)-porphyrin (IN3) or Fe(II)-porphyrin (IN3') to undergo the subsequent chain propagation process.

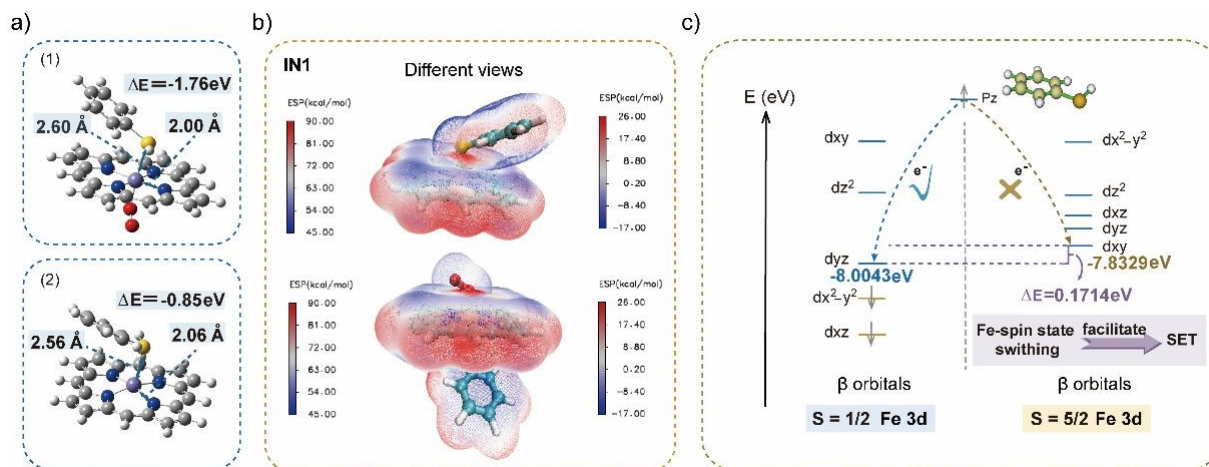


Figure 4. Theoretical calculations on the generation of RS[•]. (a) DFT optimized structures of IN1 (1) and IN1' (2). (b) Molecular electrostatic potentials of IN1. The left axis corresponds to the iron porphyrin and the right axis corresponds to the axial ligands. (c) Calculated Fe 3d orbitals of iron porphyrins with different spin states. The yellow lines represent the occupied 3d orbitals, and the blue lines represent the unoccupied 3d orbitals.

Theoretical calculations for exploring effects of spin state switching on SET

To further examine the radical initiation to obtain RS[•] and explore effects of spin state on electron transfer, the theoretical calculation was employed using density functional theory (DFT). With an unsubstituted porphyrin and thiophenol as the models, the calculations were carried out at the BP86/D ef2-TZVP level. Geometrical parameters and electronic structures of IN1 (6C with O₂) and IN1' (5C without O₂) were optimized with the Gaussian 09 program package.⁵³ In the optimized structures of IN1 and IN1', thiophenol and O₂ acted as axial ligands to coordinate with Fe(III)-porphyrin (Figure 4a). These respectively resulted in the adsorption energy of -1.76 and -0.85 eV, indicating their stable coordination to obtain intermediates. In addition, a difference of 0.04 Å in the Fe—S bond length was resulted for optimized structures of IN1 and IN1', which was attributed to the axial coordination of oxygen. Besides, the bond lengths of Fe-Npyr were 2.00 Å (for IN1) and 2.06 Å (for IN1'), which could be attributed to the low and high spin thiolate-bound complexes.^{50,54} Consequently, it can be deduced that the spin state of thiolate-coordinated Fe(III)-porphyrin was transformed to a low one with oxygen bound to the iron, which would facilitate the following reactions.

Thereafter, to further reveal the charge distribution of intermediates, the molecular electrostatic potential (MEP) maps of IN1 were computed to examine the sites of SET.⁵⁵⁻⁵⁶ As shown in Figure 4b and Figure S13, Fe(III) exhibited the positive potential with the red region, which indicated the ability of receiving electrons. Whereas both regions of -SH and

-C=C in the substrate **1** were in a negative potential (blue shed) for providing electrons. Consequently, upon the coordination between electron-rich sulfhydryl and Fe(III)-porphyrin, the electron would be transferred from the sulfhydryl group to Fe(III) for the selective RS[•] generation. This was in accordance with the significantly reduced yield of TEC reaction in CH₃OH, which acts as an axial ligand solvent with higher adsorption energy (-1.79 eV) than IN1 (-1.76 eV) (Figure S14). Therefore, CH₃OH can act as a strong coordinating solvent to compete with sulfhydryl, coordinating with Fe(III)-porphyrin to impede SET. This could also be an indirect proof for the SET-based radical initiation process.

To further explore effects of spin state and O₂ coordination on SET-based radical initiation, the Fe 3d orbitals of Fe-porphyrins with different spin states and S p orbital of substrate were calculated. Herein (Figure 4c and Figure S15), the energy of lowest unoccupied 3d orbital was calculated to evaluate the ability of electron accepting in the first SET. Considering the alpha orbitals of Fe(III) with high spin state were all occupied, the electron of sulfhydryl would be transferred into the beta orbital (E=-7.38 eV). While with O₂ coordinated, the energy of lowest unoccupied beta orbital was -8.00 eV, which was lower than the alpha one (-7.21 eV). This induced the inclined entering of electrons to the unoccupied beta orbitals. From the thermodynamic point of view, the lower energy of low spin state (-8.00 eV) than high spin state (-7.38 eV) also suggested the favourable electron transfer from sulfhydryl to Fe(III). Therefore, the SET-based radical initiation of RS[•] would be further promoted in the presence of O₂, facilitating the formation of 6C IN1 at low spin state. While



without O₂, the 5C IN1' in high spin state was obtained to limit the reaction, in accordance with the lower yield in N₂. Therefore, O₂ not only avoids the subsequent catalyst deactivation, but also plays a key role in the formation of IN1 at a low spin state to facilitate the SET-based initiation.

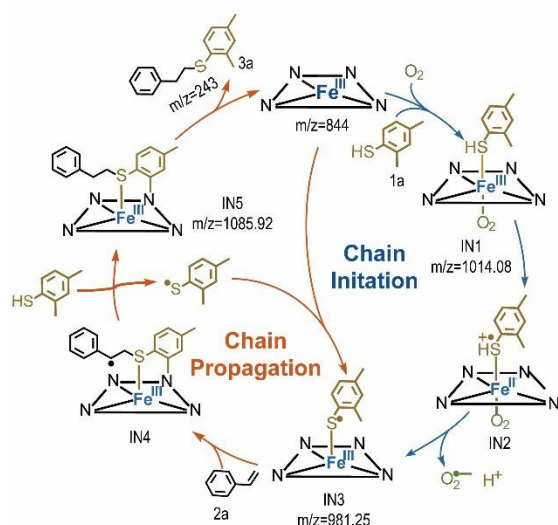


Figure 5. The mechanism of SET-initiated TEC reaction.

The mechanism of SET-initiated TEC reaction

Based on the aforementioned experimental and theoretical examinations, the mechanism of SET-initiated TEC in air can be proposed (Figure 5). Initially, the axial ligands of substrate **1a** and O₂ were coordinated with the catalyst of Fe(III)TCPP ([Fe(III)TCPP]⁺ at *m/z* 844.5) to form IN1 at the low spin state ([RSH-Fe(III)TCPP-O₂]⁺ at *m/z* 1014.1). Compared to IN1' at high spin state, the generated IN1 at the low spin state reduced the energy barrier of SET. In this way, the intramolecular selective SET was employed from sulfhydryl to Fe(III), which generated the intermediate complex of RS[•] and Fe(II) (IN2). Subsequently, Fe(II) in IN2 was oxidized by O₂ via the second SET process, forming O₂^{•-} and another intermediate of IN3 ([Fe(III)TCPP-RS[•]]⁺ at *m/z* 981.3). It should be noted that the generated O₂^{•-} can participate in the oxidation of sulfur-containing compounds, leading to the formation of sulfoxides (Figure 1b, *m/z* 259) at a relatively low abundance. Thereafter, the chain propagation would be initiated through a two-step SET-based radical initiation. This involves radical addition to the -C=C bond in substrate **2a**, generating a carbon-centered radical (IN4) that abstracts an H atom from another molecule of substrate **1a**. This induced the generation of hydrothiolated intermediate IN5 ([Fe(III)TCPP-3a]⁺ at *m/z* 1085.9) and another equivalent of RS[•]. Finally, the product ([3a+H]⁺ at *m/z* 243) was desorbed from the catalyst to complete the TEC reaction.

Besides, the generated RS[•] can be directly captured by the catalyst to obtain IN3 upon the coordination between Fe(III)TCPP and RS[•], fulfilling another run of the chain propagation. Upon this sizable Fe(III)TCPP-based coordination, bulky RS[•] species with the increased steric hindrance would endow active RS[•] with high stability for subsequent reactions.

It should be noted that a low abundance of disulfide product was also exhibited even in N₂ atmosphere (Figure S16). Consequently, the homo-coupling of bulky RS[•] species (IN3) would be restricted due to the steric hindrance, which would facilitate the coupling with the vinyl reactants. Therefore, the side reactions would be avoided upon the stabilization of radicals by the Fe(III)TCPP-based coordination, which was confirmed by the decreased yield and conversion with free Fe(III) as the catalyst (Figure S17). Consequently, the controllable SET-based initiation of RS[•] upon axial-ligand-induced switching of spin states and the subsequent selective chain propagation were revealed.

Conclusions

In summary, the axial-ligand-induced switching of spin states in Fe(III)-catalyzed TEC reaction was revealed, which facilitated the controllable generation of RS[•] via SET process. As demonstrated by AMS-based characterization and other examinations, RS[•] was demonstrated to be selectively and controllably generated via SET between substrate **1** and Fe(III)-porphyrin. The role of axial-ligand for inducing switching of transition metal's spin states was revealed, which facilitated the RS[•] radical initiation and subsequent reactions. With O₂ as another axial ligand, the thiolate-coordinated Fe(III)-porphyrin (IN1' *S* = 5/2) was transformed to low spin state (IN1 *S* = 1/2), dramatically lowering the energy barrier of SET-based radical generation. This well explains the efficient and selective C-S coupling in air. Subsequently, upon the coordination with the bulky Fe(III)-porphyrin, the RS[•] species (IN3) selectively coupled with vinyl reactant for efficient TEC reactions. Consequently, based on AMS monitoring and comprehensive examinations, the efficient and selective TEC reactions originated from spin-regulated SET-based RS[•] initiation. This work not only holds the promise for efficient and selective radical reactions upon manipulating spin states but also broadens the applications of AMS for in-depth mechanism examinations.

Data availability

All data of this study have been presented in the manuscript and ESI. †

Author contributions

J. Qin and Y. Yin conceived and designed the project; X. Guan contributed to the characterizations of products; J. Qin, Y. Yin and X. Ge conducted the calculation; M. Cao and J. Ouyang supported figure preparations. N. Na directed the whole project and acquired the funding. All authors have given approval to the manuscript.

Conflicts of interest

There are no conflicts to declare.



Acknowledgements

We gratefully acknowledge the National Natural Science Foundation of China (No. 22474010 and 22274012), the National Key Research and Development Program of China (2024YFA1509600) and the Fundamental Research Funds for the Central Universities (No.2233300007).

Notes and references

- S. Wang, S. Tang and A. Lei, *Sci. Bull.*, 2018, **63**, 1006-1009.
- H. Yi, G. Zhang, H. Wang, Z. Huang, J. Wang, A. K. Singh and A. Lei, *Chem. Rev.*, 2017, **117**, 9016-9085.
- P. Sivaguru, Z. Wang, G. Zanoni and X. Bi, *Chem. Soc. Rev.*, 2019, **48**, 2615-2656.
- W.-C. C. Lee, D.-S. Wang, Y. Zhu and X. P. Zhang, *Nat. Chem.*, 2023, **15**, 1569-1580.
- J.-R. Chen, X.-Q. Hu, L.-Q. Lu and W.-J. Xiao, *Chem. Soc. Rev.*, 2016, **45**, 2044-2056.
- M. Yan, J. C. Lo, J. T. Edwards and P. S. Baran, *J. Am. Chem. Soc.*, 2016, **138**, 12692-12714.
- P. Xu, J. Xie, D.-S. Wang and X. P. Zhang, *Nat. Chem.*, 2023, **15**, 498-507.
- Z. Huang, Y. Yang, J. Mu, G. Li, J. Han, P. Ren, J. Zhang, N. Luo, K.-L. Han and F. Wang, *Chinese J. Catal.*, 2023, **45**, 120-131.
- H.-M. Huang, P. Bellotti and F. Glorius, *Chem. Soc. Rev.*, 2020, **49**, 6186-6197.
- Q. Zhou, M. Chin, Y. Fu, P. Liu and Y. Yang, *Science*, 2021, **374**, 1612-1616.
- M. Chierchia, P. Xu, G. J. Lovinger and J. P. Morken, *Angew. Chem. Int. Ed.*, 2019, **58**, 14245-14249.
- A. Dahiya and B. K. Patel, *Chem. Rec.*, 2021, **21**, 3589-3612.
- X. Wang, J. He, Y.-N. Wang, Z. Zhao, K. Jiang, W. Yang, T. Zhang, S. Jia, K. Zhong, L. Niu and Y. Lan, *Chem. Rev.*, 2024, **124**, 10192-10280.
- M. Mato, D. Spinnato, M. Leutzsch, H. W. Moon, E. J. Reijerse and J. Cornella, *Nat. Chem.*, 2023, **15**, 1138-1145.
- S. Chen, X. Liang, S. Hu, X. Li, G. Zhang, S. Wang, L. Ma, C.-M. L. Wu, C. Zhi and J. A. Zapien, *Nano-Micro. Lett.*, 2023, **15**, 47.
- C. Zhang, X. Wang, Z. Ma, H. Yao, H. Liu, C. Li, J. Zhou, R. Xu, X. Zheng, H. Wang, Q. Li, M. Gu, H. Jiang and M. Huang, *Sci. Bull.*, 2023, **68**, 2042-2053.
- F. He, Q. Zheng, X. Yang, L. Wang, Z. Zhao, Y. Xu, L. Hu, Y. Kuang, B. Yang, Z. Li, L. Lei, M. Qiu, J. Lu and Y. Hou, *Adv Mater.*, 2023, **35**, 2304022.
- G.-Z. Huang, Y.-S. Xia, F. Yang, W.-J. Long, J.-J. Liu, J.-P. Liao, M. Zhang, J. Liu and Y.-Q. Lan, *J. Am. Chem. Soc.*, 2023, **145**, 26863-26870.
- Y. Zhang, Q. Wu, J. Z. Y. Seow, Y. Jia, X. Ren and Z. J. Xu, *Chem. Soc. Rev.*, 2024, **53**, 8123-8136.
- K. Sun, Y. Huang, Q. Wang, W. Zhao, X. Zheng, J. Jiang and H.-L. Jiang, *J. Am. Chem. Soc.*, 2024, **146**, 3241-3249.
- Q. Zhao, M. Zhang, Y. Gao, H. Dong, L. Zheng, Y. Zhang, J. Ouyang and N. Na, *J. Am. Chem. Soc.*, 2024, **146**, 14875-14888.
- B. H. Northrop and R. N. Coffey, *J. Am. Chem. Soc.*, 2012, **134**, 13804-13817.
- R. Kumar, Saima, A. Shard, N. H. Andhare, Richa and A. K. Sinha, *Angew. Chem. Int. Ed.*, 2015, **54**, 828-832.
- Q. Xiao, H. Zhang, J.-H. Li, J.-X. Jian, Q.-X. Tong and J.-J. Zhong, *Org. Lett.*, 2021, **23**, 3604-3609.
- R.-J. Zhang, X.-R. Li, R.-B. Liang, Y. Xiao, Q.-X. Tong, J.-J. Zhong and L.-Z. Wu, *Org. Lett.*, 2024, **26**, 591-596.
- Z. Wu and D. A. Pratt, *Nat. Rev. Chem.*, 2023, **7**, 573-589.
- J. Twilton, C. Le, P. Zhang, M. H. Shaw, R. W. Evans and D. W. C. MacMillan, *Nat. Rev. Chem.*, 2017, **1**, 0052.
- C. Ma, P. Fang, Z.-R. Liu, S.-S. Xu, K. Xu, X. Cheng, A. Lei, H.-C. Xu, C. Zeng and T.-S. Mei, *Sci. Bull.*, 2021, **66**, 2412-2429.
- N. Taniguchi, *ChemistrySelect*, 2018, **3**, 6209-6213.
- A. K. Sinha and D. Equbal, *Asian J. Org. Chem.*, 2019, **8**, 32-47.
- S. Mondal, F. Dumur, D. Gimes, M. P. Sibi, M. P. Bertrand and M. Nechab, *Chem. Rev.*, 2022, **122**, 5842-5976.
- Y. Wang, Y. Zhou, W. Sun, X. Wang, J. Yao and H. Li, *Adv. Sci.*, 2024, **11**, 2402890.
- H. Yang, E. C. McDaniel, S. Impano, A. S. Byer, R. J. Jodts, K. Yokoyama, W. E. Broderick, J. B. Broderick and B. M. Hoffman, *J. Am. Chem. Soc.*, 2019, **141**, 12139-12146.
- P. J. H. Williams, G. A. Boustead, D. E. Heard, P. W. Seakins, A. R. Rickard and V. Chechik, *J. Am. Chem. Soc.*, 2022, **144**, 15969-15976.
- W. G. Walls, A. L. Vagstad, T. Delridge, J. Piel, W. E. Broderick and J. B. Broderick, *J. Am. Chem. Soc.*, 2024, **146**, 5550-5559.
- X. Ge, Y. Yin, J. Sun, J. Ouyang and N. Na, *Chem. Sci.*, 2023, **14**, 2229-2236.
- H. Lu, Y. Yin, J. Sun, W. Li, X. Shen, X. Feng, J. Ouyang and N. Na, *Chinese Chem. Lett.*, 2021, **32**, 3457-3462.
- S. Jin, H. Chen, X. Yuan, D. Xing, R. Wang, L. Zhao, D. Zhang, C. Gong, C. Zhu, X. Gao, Y. Chen and X. Zhang, *JACS Au*, 2023, **3**, 1563-1571.
- X. Li, X. Nong, C. Zhu, X. Gao, H. Chen, X. Yuan, D. Xing, L. Liu, C. Liang, D. Zhang and X. Zhang, *J. Am. Chem. Soc.*, 2024, **146**, 29267-29271.
- K. Mittra, A. Singha and A. Dey, *Inorg. Chem.*, 2017, **56**, 3916-3925.
- N. Taniguchi and K. Kitayama, *Synlett*, 2018, **29**, 2712-2716.
- C. Xu, Y. Pan, G. Wan, H. Liu, L. Wang, H. Zhou, S.-H. Yu and H.-L. Jiang, *J. Am. Chem. Soc.*, 2019, **141**, 19110-19117.
- S. Guo, G. Zhang, Y. Guo and J. C. Yu, *Carbon*, 2013, **60**, 437-444.
- L. Geng, M. Zhang, W. Zhang, M. Jia, W. Yan and G. Liu, *Catal. Sci Technol.*, 2015, **5**, 3097-3102.
- Q. Zhao, L. Zheng, Y. Gao, J. Li, J. Wei, M. Zhang, J. Sun, J. Ouyang and N. Na, *J. Am. Chem. Soc.*, 2023, **145**, 12586-12600.
- H. Di Wang, P. J. Pagano, Y. Du, A. J. Cayatte, M. T. Quinn, P. Brecher and R. A. Cohen, *Circ. Res.*, 1998, **82**, 810-818.
- H.-S. Hsieh, R. Wu and C. T. Jafvert, *Environ. Sci. Technol.*, 2014, **48**, 11330-11336.
- A. Gemenetzi, P. Stathi, Y. Deligiannakis and M. Louloudi, *Chem. Phys. Lett.*, 2021, **764**.
- W. Shi, L. Cao, H. Zhang, X. Zhou, B. An, Z. Lin, R. Dai, J. Li, C. Wang and W. Lin, *Angew. Chem. Int. Ed.*, 2017, **56**, 9704-9709.
- P. K. Das, S. Chatterjee, S. Samanta and A. Dey, *Inorg. Chem.*, 2012, **51**, 10704-10714.
- S. Samanta, S. Sengupta, S. Biswas, S. Ghosh, S. Barman and A. Dey, *J. Am. Chem. Soc.*, 2023, **145**, 26477-26486.
- N. Ueyama, N. Nishikawa, Y. Yamada, T. Okamura and A. Nakamura, *J. Am. Chem. Soc.*, 1996, **118**, 12826-12827.
- M. J. Frisch, G. W. T., H. B. Schlegel, G. E. Scuseria, M. A. Robb, J. R. Cheeseman, G. Scalmani, V. Barone, B. Mennucci, G. A. Petersson, H. Nakatsuji, M. Caricato, X. Li, H. P. Hratchian, A. F. Izmaylov, J. Bloino, G. Zheng, J. L. Sonnenberg, M. Hada, M. Ehara, K. Toyota, R. Fukuda, J. Hasegawa, M. Ishida, T. Nakajima, Y. Honda, O. Kitao, H. Nakai, T. Vreven, J. A. Montgomery, Jr., J. E. Peralta, F. Ogliaro, M. Bearpark, J. J. Heyd, E. Brothers, K. N. Kudin, V. N. Staroverov, R. Kobayashi, J. Normand, K. Raghavachari, A. Rendell, J. C. Burant, S. S. Iyengar, J. Tomasi, M. Cossi, N. Rega, J. M. Millam, M. Klene, J. E. Knox, J. B. Cross, V. Bakken, C. Adamo, J. Jaramillo, R. Gomperts, R. E. Stratmann, O. Yazyev, A. J. Austin, R. Cammi, C. Pomelli, J. W. Ochterski, R. L. Martin, K. Morokuma, V. G. Zakrzewski, G. A. Voth, P.



Salvador, J. J. Dannenberg, S. Dapprich, A. D. Daniels, Ö. Farkas, J. B. Foresman, J. V. Ortiz, J. Cioslowski and D. J. Fox, *Gaussian 09, Revision D.01*, Gaussian Inc., Wallingford, CT, 2009.

54 N. Suzuki, T. Higuchi, Y. Urano, K. Kikuchi, H. Uekusa, Y. Ohashi, T. Uchida, T. Kitagawa and T. Nagano, *J. Am. Chem. Soc.*, 1999, **121**, 11571-11572.

55 T. Lu and F. Chen, *J. Comput. Chem.*, 2012, **33**, 580-592.

56 J. Zhang and T. Lu, *Phys. Chem. Chem. Phys.*, 2021, **23**, 20323-20328.

View Article Online
DOI: 10.1039/D5SC02194D



All data of this study have been presented in the manuscript and ESI.

[View Article Online](#)

DOI: 10.1039/D5SC02194D

